

**Nonunique and nonuniform mapping in few-body Coulomb-explosion imaging**A. M. Saylor,<sup>1,2,3</sup> E. Eckner,<sup>1</sup> J. McKenna,<sup>2</sup> B. D. Esry,<sup>2</sup> K. D. Carnes,<sup>2</sup> I. Ben-Itzhak,<sup>2</sup> and G. G. Paulus<sup>1,3</sup><sup>1</sup>*Institut für Optik und Quantenelektronik Max-Wien-Platz 1, 07743 Jena, Germany*<sup>2</sup>*J. R. Macdonald Laboratory, Department of Physics, Kansas State University, Manhattan, Kansas 66506, USA*<sup>3</sup>*Helmholtz Institut Jena, 07743 Jena, Germany*

(Received 15 June 2017; revised manuscript received 14 December 2017; published 28 March 2018)

Much of our knowledge of molecular geometry and interaction dynamics comes from indirect measurements of the molecular fragments following breakup. This technique—Coulomb-explosion imaging (CEI), i.e., determining the initial molecular configuration of a system from the momenta of the resulting fragments using knowledge of the particle interactions—is one of the fundamental tools of molecular physics. Moreover, CEI has been a staple of molecular studies for decades. Here we show that one often cannot assign a unique initial configuration to the few-body breakup of a polyatomic molecule given the measurement of the resulting fragments' momenta. Specifically, multiple initial configurations can result in identical momenta for a molecule breaking into three or more parts. Further, the nonunique and nonuniform mapping from the initial configuration to the measured momenta also significantly complicates the determination of molecular alignment at the time of breakup.

DOI: [10.1103/PhysRevA.97.033412](https://doi.org/10.1103/PhysRevA.97.033412)**I. INTRODUCTION**

In the quest to understand molecular geometry and dynamics, a typical ploy is to break the molecule and determine the initial configuration from the asymptotic momenta of the resulting fragments. This is done in a three-step process. First, the molecule is instantly moved to an unbound state, e.g., by stripping electrons using thin foils [1–8], highly charged ions [9–15], electron impact [16], or photofragmentation [17–27], so that the repulsive force of the nuclei outweighs the binding force [28]. Second, the measured impact times and positions of the fragments at the detector are used to determine the final momenta of the fragments [29–31]. Third, classical physics is used to “run the clock backwards” to the instant the sequence began. This technique—Coulomb-explosion imaging (CEI)—has been a workhorse of experimental physics and chemistry for decades [1–27] and continues to play a vital role in cutting-edge research today (e.g., see Refs. [32–34]).

Further, CEI is inexorably linked to our understanding of molecular physics as it has shed light upon such fundamental processes as the Franck-Condon principle [16], dissociative recombination [35–42], the breakdown of the Born-Oppenheimer approximation [43], and reaction pathways and dynamics in collision and photoinduced dissociation [44], to name a few. Additionally, CEI has evolved to include the detection of multiple ionic fragments as well as electrons, neutrals, and photons. Further, it remains a standard for the interpretation of a vast range of measurements to this day, e.g., recoil-ion momentum spectroscopy (RIMS) [29], cold-target recoil-ion momentum spectroscopy (COLTRIMS) [29–31], photoelectron-photoion-photoion coincidence (PEPIPICO) [45–49], and molecular-ion-beam dissociation imaging (MDI) [50].

For example, energy conservation dictates that instantly removing two electrons from H<sub>2</sub> with an internuclear separation of  $R$  and no initial momentum due to rovibrational

motion, referred to later as “initial momentum” for brevity, will result in two protons flying back to back [16], each with a final energy of  $0.5/R$  [51]. Moreover, the converse must be true, and protons measured with a combined kinetic energy release (KER) must have come from a H<sub>2</sub> molecule with an internuclear separation of  $R = 1/\text{KER}$ . Furthermore, this holds for any classical treatment of two-body fragmentation where the interaction between the fragments is known and the final momenta are measured. Note that although the nuclei are treated as classical particles with no uncertainty in position or velocity, one can obtain quantum mechanical information such as the distribution of internuclear separations,  $|\Psi(R)|^2$  [4,5,16,17,52]. Although energy conservation is used in this example, one can also use time evolution to determine the initial configuration. That is to say, one can either search through the initial configurations until time evolution produces the measured momenta, i.e., in the aforementioned case try different initial  $R$  values until the final conditions are best fulfilled, or reverse the final velocities and fly the fragments back in time to their initial positions. The latter is typically not feasible as small deviations, at the laboratory scale, in the measured final parameters result in large deviations in the initial distances on the atomic scale when performing a reverse time evolution calculation.

Unlike the two-body scenario, in the case of  $n$ -body breakup ( $n \geq 3$ ), energy conservation alone is not sufficient for the reconstruction of the initial conditions. A common assumption of  $n$ -body CEI is that the final momentum configuration is synonymous with the initial spatial configuration. As an example, in our measurements of three-body breakup of D<sub>3</sub><sup>3+</sup>, see Fig. 5 in Ref. [53] and Fig. 15 in Ref. [54], a Dalitz plot showing the energy sharing of the (D<sub>3</sub><sup>3+</sup> → D<sup>+</sup> + D<sup>+</sup> + D<sup>+</sup>) fragments resulting from Coulomb explosion, taken at face value, could lead one to erroneous conclusions about the initial configuration as is discussed below. Moreover, although the classical problem is unique and time-reversal invariant given

a simultaneous determination of the exact time, position, and momentum upon impact at the detector, typical measurements only determine the position and time of the particle impacts and infer the momentum from this. Thus, there is insufficient information for a unique mapping from the measured quantities to the initial configuration, and one is forced to search for the initial geometry that will produce the final results.

This problem has been addressed for the bending angle of symmetric molecules, e.g.,  $\text{NH}_2$ ,  $\text{H}_2\text{O}$ , and  $\text{CH}_2$  [55], using an algorithm, which starts with the measured distribution and converges to an initial distribution of configurations that is consistent with, but not necessarily unique to, the measured distributions [56]. However, this analysis is done for symmetric isosceles configurations assumed to be obtuse and does not address in detail why there are degeneracies, where the degeneracies lie, the order of the degeneracy, when these degeneracies can be avoided or excluded, and when they cannot.

In this paper, we show that there are often multiple initial geometries that yield the same measured momenta, i.e., the final measured momenta are not unique to a single initial configuration. Additionally, the Coulomb-explosion process results in a nonuniform mapping of initial spatial configurations onto final momentum configurations and a rotation of the molecular frame.

## II. THREE-BODY COULOMB-EXPLOSION IMAGING

The ideal place to begin an examination of polyatomic CEI is with the simplest possible system— $\text{H}_3^+ \rightarrow \text{H}_3^{3+} + 2e^- \rightarrow 3\text{H}^+ + 2e^-$ , where the first double-ionization step is assumed to be instantaneous, the free electrons are assumed to not play a role, and the initial momenta of the protons are assumed to be zero. This system is ideal since (i) the ground state of the initial molecule,  $\text{H}_3^+$ , is an equilateral triangle [57], (ii) the force between the fragments is pure Coulomb repulsion,  $1/R_{ij}^2$ , and (iii) the molecule is important as a benchmark for molecular interactions and calculations [53,54,58–62] and plays a central role in interstellar chemistry [63–65].

Three examples are shown in Fig. 1 to illustrate the Coulomb explosion and define the coordinates. The first row shows a molecule starting in an equilateral configuration described by the internuclear distances,  $R_{ij}$ , and the corresponding angles,  $\alpha_i$ . After removal of all the electrons, the fragments will all gain the same magnitude momentum,  $|p_i|$ , and the momenta vectors will be separated by the angles,  $\gamma_{ij}$ . To more consistently link the initial configuration to the final measured momenta, we choose to connect the ends of the momentum vectors to circumscribe a triangle with angles,  $\beta_i$ , which contain equivalent information. Unsurprisingly, the initial equilateral configuration,  $\alpha \equiv [\alpha_1, \alpha_2, \alpha_3] = [60^\circ, 60^\circ, 60^\circ]$ , leads to an equilateral final momentum configuration,  $\beta \equiv (\beta_1, \beta_2, \beta_3) = (60^\circ, 60^\circ, 60^\circ)$ . Note that the overall size of the initial configuration does not affect the initial or final angles.

In the middle row, the same information is shown for an obtuse isosceles initial configuration,  $\alpha = [13^\circ, 154^\circ, 13^\circ]$ , that results in an obtuse isosceles final momentum configuration,  $\beta = (40^\circ, 100^\circ, 40^\circ)$ . The final row shows the information for an acute isosceles initial configuration,  $\alpha = [81^\circ, 18^\circ, 81^\circ]$ , that results in the same obtuse isosceles final momentum

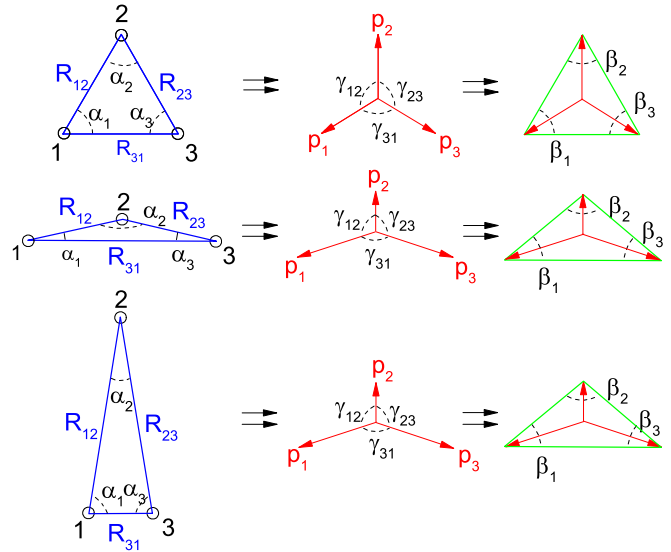


FIG. 1. Examples of three-body Coulomb explosions with equal masses. Top row: An equilateral configuration,  $\alpha \equiv [\alpha_1, \alpha_2, \alpha_3] = [60^\circ, 60^\circ, 60^\circ]$ , results in equal magnitude momenta,  $|p_i|$ , separated by  $\gamma_i = 120^\circ$ . Circumscribing the momentum vectors with a triangle results in the measurable momentum configuration  $\beta \equiv (\beta_1, \beta_2, \beta_3) = (60^\circ, 60^\circ, 60^\circ)$ . Middle row: An obtuse isosceles configuration,  $\alpha = [13^\circ, 154^\circ, 13^\circ]$ , resulting in an obtuse isosceles momentum configuration,  $\beta = (40^\circ, 100^\circ, 40^\circ)$ . Bottom row: An acute isosceles configuration,  $\alpha = [81^\circ, 18^\circ, 81^\circ]$ , resulting in the same obtuse isosceles momentum configuration,  $\beta = (40^\circ, 100^\circ, 40^\circ)$ , as above. See text for details.

configuration as the previous example,  $\beta = (40^\circ, 100^\circ, 40^\circ)$ . This is because the two protons starting closer together, labeled 1 and 3, strongly repel each other and quickly gain momentum and fly apart while the other proton, labeled 2, gains relatively little momentum. This shows both that the initial spatial configuration does not necessarily match the final momentum configuration and that a particular final momentum configuration does not necessarily uniquely correspond to a single initial configuration.

To examine this phenomenon in depth, we determine the final momentum configurations for *all* initial configurations (see Fig. 2). The final momentum configuration angles,  $(\beta_1, \beta_2, \beta_3)$ , are encoded in the color (red, green, blue) for each initial configuration,  $[\alpha_1, \alpha_2, \alpha_3]$ . Note that  $\alpha_3$  is not shown since  $\alpha_3 = 180^\circ - \alpha_2 - \alpha_1$ . The isosceles configurations shown in Fig. 1 are marked with arrows and connected to the identical final momentum configuration. Note that it is immediately apparent that the mapping from the initial configuration to the final momentum configuration,  $\alpha \rightarrow \beta$ , is neither uniform nor always unique.

An alternative way to display this information is as a contour map of the final momentum configuration (see Fig. 3). This displays the same information as Fig. 2 but allows for a more quantitative view. Here one sees that the equilateral final momentum configuration,  $\beta = (60^\circ, 60^\circ, 60^\circ)$ , is not unique to an initial equilateral configuration,  $\alpha = [60^\circ, 60^\circ, 60^\circ]$ . Rather, four initial configurations lead to this final momentum configuration, namely the equilateral triangle  $\alpha = [60^\circ, 60^\circ, 60^\circ]$  and the three permutations of  $\alpha = [40^\circ, 40^\circ, 100^\circ]$  obtuse isosceles

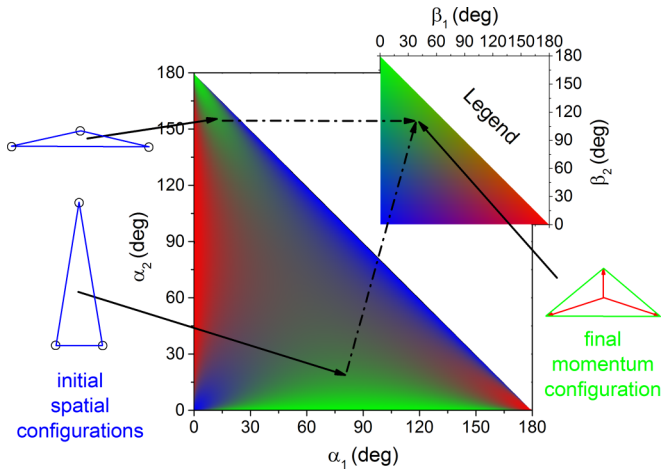


FIG. 2. The final momentum configuration,  $(\beta_1, \beta_2, \beta_3)$ , for all possible starting configurations,  $[\alpha_1, \alpha_2, \alpha_3]$ , where all configurations have the same total energy. The  $\beta$  angles are encoded in the red-green-blue color value as shown in the legend. In other words, one chooses the initial configuration angles, i.e.,  $\alpha_1$  and  $\alpha_2$ , and finds the color at the corresponding point. Then one looks for the same color in the legend and reads the final momentum configuration angles,  $\beta_1$  and  $\beta_2$ . The two isosceles lower examples shown in Fig. 1 are pointed out for reference. Both positions have the same greenish color and thus the same final momentum configuration. Note that the mapping is highly nonlinear and often not unique. See text for details and Fig. 3 for alternative representation.

triangle (see black circles in Fig. 3). Note that although the asymptotic position of the fragments is different for the initial configurations, the differences are on the scale of the initial molecular configuration, i.e., a few atomic units, which cannot be detected using CEI. That is to say, measurements of molecular fragments typically take place in the laboratory a few microseconds after fragmentation resulting in distances of a few millimeters with a measurement precision of a few micrometers in space and a few hundred picoseconds in time, which means that only the asymptotic momentum is accessible while atomic scale deviations in position are imperceptible within the measurement precision. Therefore, there are four initial configurations, which result in all three fragments having the same final measured equilateral momentum configuration.

### III. RESULTS AND DISCUSSION

#### A. Nonunique mapping

Note that the angular representation of the configuration is chosen here, since in this representation the overall mass, charge, and scale of the initial configuration *do not* affect the final momentum configuration. For example, equally scaling the charge and/or mass of all the fragments or changing the size of the initial configuration does not change the final momentum configuration angles, only the magnitudes of the momenta change. Thus, the same configuration map can be used for other symmetric triatomics, e.g., ozone ( $O_3$ ) with an initial configuration of  $\alpha = [31.6^\circ, 31.6^\circ, 116.8^\circ]$ . This configuration is indistinguishable by CEI from initial configurations of  $\alpha = [67^\circ, 67^\circ, 46^\circ]$ ,  $\alpha = [51^\circ, 88^\circ, 41^\circ]$ , and  $\alpha = [88^\circ, 51^\circ, 41^\circ]$ , as

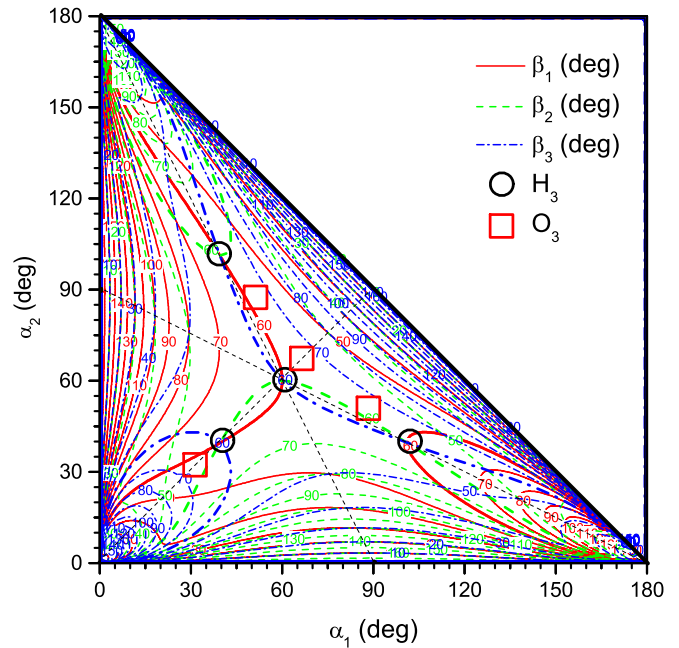


FIG. 3. The same information shown in Fig. 2 displayed as a contour map. Isosceles configurations are marked by black dashed lines and  $\beta = 60^\circ$  contours are slightly bolder to guide the eye. Circles denote initial configurations leading to  $\beta = (60^\circ, 60^\circ, 60^\circ)$ . Squares denote the initial configuration of ozone ( $O_3$ ),  $\alpha = [31.6^\circ, 31.6^\circ, 116.8^\circ]$ , and three other initial configurations, which all lead to the same final momenta,  $\beta = (57^\circ, 57^\circ, 66^\circ)$ . See text for details.

all lead to the same final momenta,  $\beta = (57^\circ, 57^\circ, 66^\circ)$ , marked by squares in Fig. 3.

In some cases one may argue that this lack of uniqueness is not important—(i) when the difference between the indistinguishable initial configurations is negligible or (ii) when the difference between the indistinguishable initial configurations is large enough that it allows exclusion of all but one configuration on other grounds; e.g., if one knows the initial  $H_3^+$  vibrational wave function, then certain exotic configurations with near zero probability could be excluded. However, the ground-state vibrational eigenfunction for  $H_3^+$  has a wide distribution centered around the equilibrium configuration [57,66], and most ion sources produce vibrationally excited  $H_3^+$  with a broad population peaked around  $\nu = 6$  [67]. Thus, there is a non-negligible probability for all four of the initial configurations marked by circles in Fig. 3 that lead to the same equilateral momentum configuration. Therefore, one cannot rule out any of the initial configurations if the equilateral momentum configuration is measured.

#### B. Nonuniform mapping

In addition to degenerate initial configurations, it is also apparent from Fig. 2 that the initial configurations are nonuniformly mapped onto final configurations; i.e., the Jacobian determinant is not constant. This means that the distribution of final momentum configurations is skewed with respect to the distribution of initial spatial configurations. This is illustrated in Fig. 4 for an isotropic distribution of initial

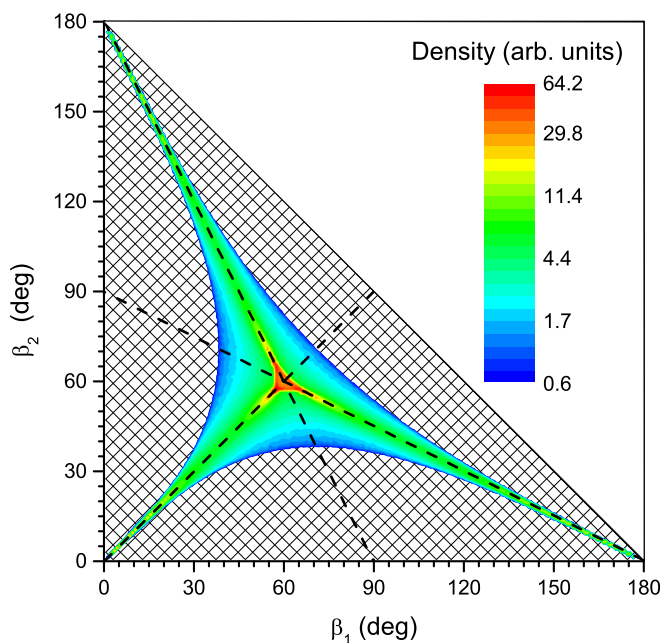


FIG. 4. The density of the final momentum configurations resulting from a uniform distribution of initial configurations (the hashed triangle) plotted on a logarithmic scale. Note that the density is pushed towards symmetric configurations. See text for details.

configurations in angular space. Note that the final distribution is strongly skewed towards obtuse symmetric configurations while strongly asymmetric and acute final configurations are nearly impossible. Although this may be initially unexpected, it is not surprising upon consideration of the dynamics of Coulomb explosion discussed above and has been taken into account in the analysis of previous CEI measurements of molecular bending angles [55,56].

### C. Alignment distortion

The alignment of a molecule is also of interest in many processes, e.g., preferential laser-induced fragmentation with respect to the laser polarization [54] or preferential collision-induced fragmentation with respect to an incident particle velocity [68]. In addition to, and independent of, the change in shape, here too there is a nonuniform mapping from the initial to final states. Namely, assuming no initial angular momentum, determining the principle axes of the inertia tensor, defining the principle axis about which inertia is minimized to be the primary axis, and treating the final momentum vectors equivalently to position vectors, one obtains the rotation of the primary axis in the molecular plane shown in Fig. 5. Thus, one cannot assume that alignment of the final momentum vectors with an outside coordinate system, e.g., a laser polarization or particle velocity, necessitates the alignment of the initial configuration in the same direction.

### D. Mass-asymmetric molecules

To determine if these phenomena are unique to and only significant for  $\text{H}_3^+$ , which is a very special polyatomic molecule with equal masses and an initial distribution peaked at

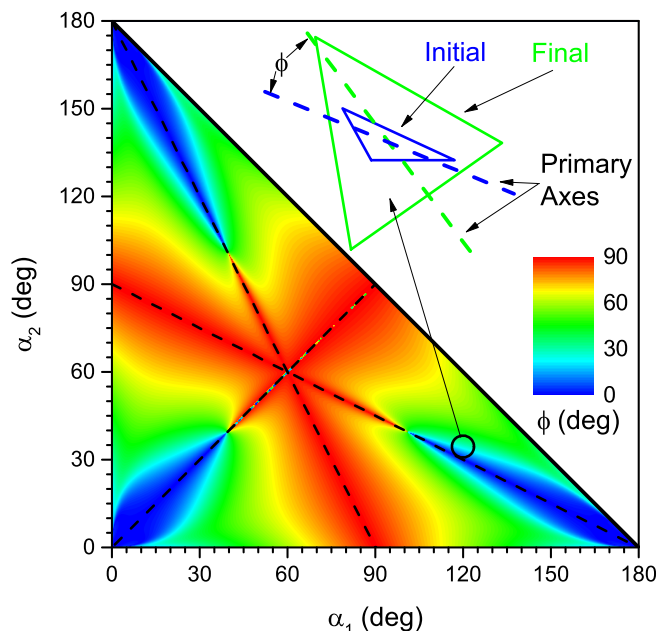


FIG. 5. The rotation,  $\phi$ , of the primary axis of the inertia tensor from the initial to the final configuration. Inset: An example of this rotation for  $\alpha = [120^\circ, 35^\circ, 25^\circ] \rightarrow \beta = (65^\circ, 51^\circ, 64^\circ)$ . See text for details.

the equilateral configuration, additional triatomic systems are examined. Figure 6 displays a plot of the final configuration of the fragments for all possible starting configurations for  $\text{H}_2\text{O}^{3+}$  under the assumption that the interaction is purely Coulombic. We find that the details of the mapping differ from the homonuclear case, but the general features are similar

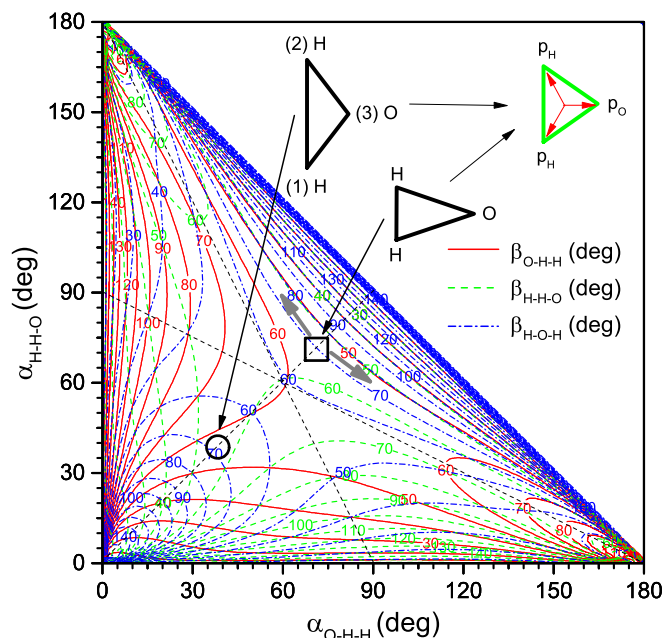


FIG. 6. Plot of the final configuration of the fragments for all possible starting configurations for  $\text{H}_2\text{O}^{3+}$ . See text for details.

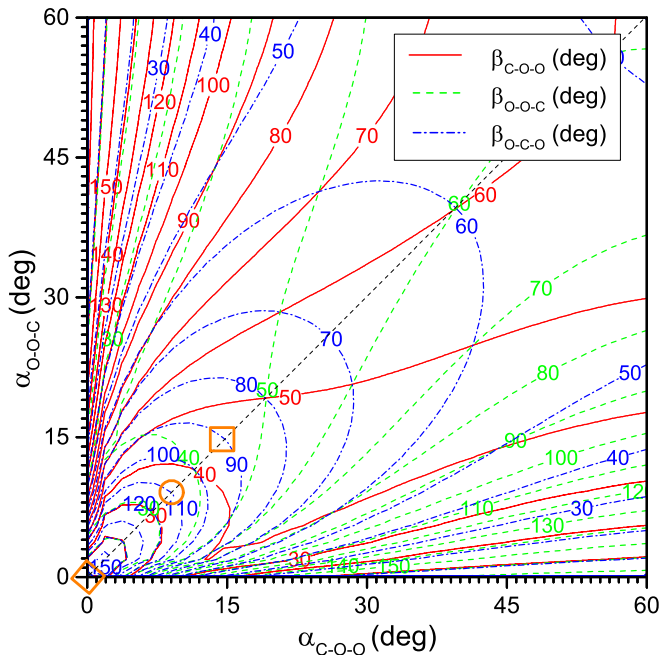


FIG. 7. Plot of the final configuration of the fragments for all possible starting configurations for  $\text{CO}_2^{3+}$  zoomed into the near-linear configurations. See text for details.

and the aforementioned phenomena are indeed significant for triatomic molecules in general.

The ground state of water has an H-O-H angle of  $104.5^\circ$ . As shown in Fig. 6, this initial configuration (circle) is indistinguishable from a configuration with an H-O-H angle of  $37^\circ$  (square) as both give a final momentum configuration of  $\beta = (55^\circ, 55^\circ, 70^\circ)$ . Furthermore, there is a very broad range of initial configurations resulting in very similar final configurations, i.e., all those configurations where the three different color contour lines follow the same path with an H-O-H angle of  $\sim 37^\circ$  (gray arrows). This makes the initial configuration almost impossible to distinguish. In the case of  $\text{H}_2\text{O}^+$ , the  $\sim 37^\circ$  configurations are so far from the predicted  $104.5^\circ$  configuration that these degeneracies can likely be ruled out. Nevertheless, it illustrates how large regions of the initial configuration space can be indistinguishable within typical experimental precision, and additional assumptions must be relied upon to exclude possible solutions.

Doing the same analysis for the ground state of carbon dioxide, which has an equally spaced *linear* O-C-O configuration, we find that it is difficult to distinguish from unequally spaced linear configurations as the two outer  $\text{O}^+$  ions tend to center the  $\text{C}^+$  ion; i.e., the  $\text{O}^+$  momenta tend toward being mirrored about a near-zero  $\text{C}^+$  momentum (see Fig. 7). Additionally, when the alignment is not perfectly linear, the obtuse angle in initial configurations is reduced in the final configuration for the reasons discussed above. However, the initial configuration space around a linear configuration is expanded onto a much larger final configuration space, which could make measuring small deviations from a linear configuration much easier given a proper treatment of the Coulomb explosion. For example, the diamond, the circle, and the square in Fig. 7 mark the  $\alpha = [0^\circ, 0^\circ, 180^\circ]$ ,  $[9^\circ, 9^\circ, 162^\circ]$ , and  $[15^\circ, 15^\circ, 150^\circ]$  configurations,

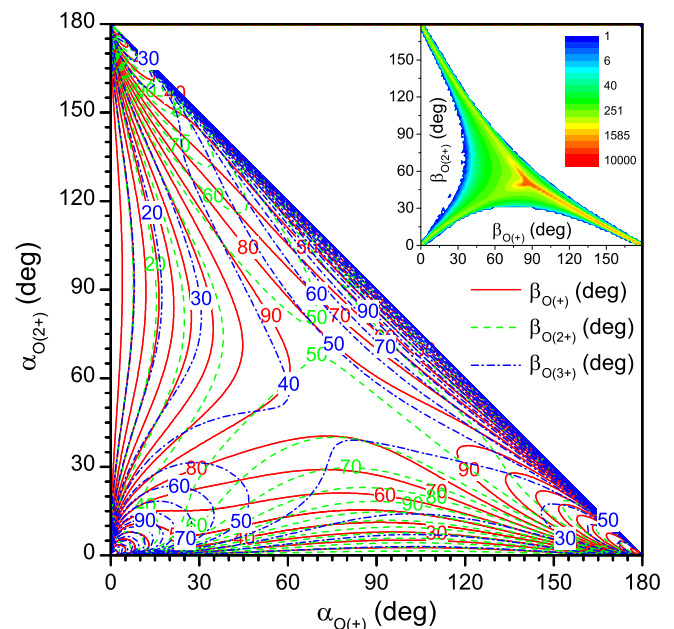


FIG. 8. Plot of the final configuration of the fragments for all possible starting configurations for  $\text{O}_3^{6+} \rightarrow \text{O}^+ + \text{O}^{2+} + \text{O}^{3+}$ . Inset: The density of the final momentum configurations resulting from a uniform distribution of initial configurations plotted on a logarithmic scale. See text for details.

respectively. These result in the momentum configurations of  $\beta = (0^\circ, 0^\circ, 180^\circ)$ ,  $(35^\circ, 35^\circ, 110^\circ)$ , and  $(45^\circ, 45^\circ, 90^\circ)$ , respectively. In other words, a small deviation from linear will give the  $\text{C}^+$  ion a large kick from the  $\text{O}^+$  ions effectively amplifying the initial angle. In addition to  $\alpha \simeq [0^\circ, 0^\circ, 180^\circ]$ , the linear configuration, extremely acute triangles  $\alpha \simeq [90^\circ, 90^\circ, 0^\circ]$  will also produce identical final configurations.

### E. Charge-asymmetric molecules

To illustrate the behavior of an asymmetric breakup, we plot the final momentum configurations for all possible initial configurations of the breakup,  $\text{O}_3^{6+} \rightarrow \text{O}^+ + \text{O}^{2+} + \text{O}^{3+}$ , in Fig. 8. One sees that in general the highest charge gains the largest momentum. For example, starting with an equilateral configuration, the  $\text{O}^{3+}$  ion gains the most momentum, which results in the smallest angle, i.e.,  $[\alpha_{\text{O}^+}, \alpha_{\text{O}^{2+}}, \alpha_{\text{O}^{3+}}] = [60^\circ, 60^\circ, 60^\circ] \rightarrow (90^\circ, 50^\circ, 40^\circ) = (\beta_{\text{O}^+}, \beta_{\text{O}^{2+}}, \beta_{\text{O}^{3+}})$ . This also skews the peak in the density of final states, resulting from a uniform distribution of initial states, to around  $(\beta_{\text{O}^+}, \beta_{\text{O}^{2+}}, \beta_{\text{O}^{3+}}) \simeq (86^\circ, 51^\circ, 43^\circ)$ .

Note that the effects of the remaining electrons on the interactions, i.e., a not purely Coulombic Born-Oppenheimer surface, have not been included in the examples discussed above. These interactions further complicate the problem and introduce additional degeneracies. When these interactions are included one can no longer only consider the initial angular configuration of the molecule. All possible bond lengths which match the measured kinetic energy release must also be considered. Moreover, initial velocities have also been excluded from the discussion above. Again, this significantly complicates the problem of determining the initial configuration and alignment

from the final momentum configuration, i.e., the measured quantities in CEI.

#### IV. CONCLUSIONS

In conclusion, we have shown that the measured configuration of the fragments of a polyatomic molecule do not accurately reflect the initial configuration of that molecule, except for two-body breakup under the assumption of zero initial momentum and a purely Coulombic effective two-body potential. Further, Coulomb explosion imaging (CEI) often does not yield a unique solution for the initial configuration of polyatomic molecules even if one neglects the interaction of the remaining electrons and the initial velocity distribution. Moreover, both the alignment of the molecule and the distribution of configurations are skewed by the Coulomb-explosion process. These problems greatly increase with the number of nuclei and the inclusion of electron interactions and initial velocity distributions.

Therefore, for the most part, the dream of reconstructing the initial configuration of a large molecule from the measured momenta of all the ionic fragments is simply unobtainable. In most situations CEI can only provide a verification of a predicted initial distribution of configurations and not an unambiguous determination of that configuration. Regardless, one must account for the limitations and effects discussed herein to properly interpret such measurements.

#### ACKNOWLEDGMENTS

We acknowledge fruitful discussions with L. Weaver. This work was realized with Grant No. PA730/4 from the German Research Foundation (DFG) and within the Transregio 18 (DFG) and was supported by the Chemical Sciences, Geosciences, and Biosciences Division, Office of Basic Energy Sciences, Office of Science, U.S. Department of Energy under Grant No. DE-FG02-86ER13491.

- 
- [1] Z. Vager, R. Naaman, and E. P. Kanter, *Science* **244**, 426 (1989).
- [2] E. P. Kanter, Z. Vager, G. Both, and D. Zajfman, *J. Chem. Phys.* **85**, 7487 (1986).
- [3] Z. Vager, E. P. Kanter, G. Both, P. J. Cooney, A. Faibis, W. Koenig, B. J. Zabransky, and D. Zajfman, *Phys. Rev. Lett.* **57**, 2793 (1986).
- [4] Z. Vager, T. Graber, E. P. Kanter, and D. Zajfman, *Phys. Rev. Lett.* **70**, 3549 (1993).
- [5] A. Belkacem, E. P. Kanter, R. E. Mitchell, Z. Vager, and B. J. Zabransky, *Phys. Rev. Lett.* **63**, 2555 (1989).
- [6] D. Zajfman, A. Belkacem, T. Graber, E. P. Kanter, R. E. Mitchell, R. Naaman, Z. Vager, and B. J. Zabransky, *J. Chem. Phys.* **94**, 2543 (1991).
- [7] D. Zajfman, E. P. Kanter, Z. Vager, and J. Zajfman, *Phys. Rev. A* **43**, 1608 (1991).
- [8] A. Breskin, A. Faibis, G. Goldring, M. Hass, R. Kaim, Z. Vager, and N. Zwang, *Phys. Rev. Lett.* **42**, 369 (1979).
- [9] V. Horvat, O. Heber, R. Watson, R. Parameswaran, and J. M. Blackadar, *Nucl. Instrum. Methods Phys. Res., Sect. B* **99**, 94 (1995).
- [10] B. Siegmann, U. Werner, R. Mann, N. M. Kabachnik, and H. O. Lutz, *Phys. Rev. A* **62**, 022718 (2000).
- [11] U. Werner, K. Beckord, J. Becker, and H. O. Lutz, *Phys. Rev. Lett.* **74**, 1962 (1995).
- [12] B. Siegmann, U. Werner, H. O. Lutz, and R. Mann, *J. Phys. B: At. Mol. Phys.* **34**, L587 (2001).
- [13] I. Ali, R. D. DuBois, C. L. Cocke, S. Hagmann, C. R. Feeler, and R. E. Olson, *Phys. Rev. A* **64**, 022712 (2001).
- [14] T. Kitamura, T. Nishide, H. Shiromaru, Y. Achiba, and N. Kobayashi, *J. Chem. Phys.* **115**, 5 (2001).
- [15] F. Frémont, C. Bedouet, M. Tarisien, L. Adoui, A. Cassimi, A. Dubois, J.-Y. Chesnel, and X. Husson, *J. Phys. B: At. Mol. Phys.* **33**, L249 (2000).
- [16] K. E. McCulloh and H. M. Rosenstock, *J. Chem. Phys.* **48**, 2084 (1968).
- [17] W. Koot, W. J. van der Zande, and J. Los, *Phys. Rev. Lett.* **58**, 2746 (1987).
- [18] W. Koot, W. J. van der Zande, P. H. P. Post, and J. Los, *J. Chem. Phys.* **90**, 4826 (1989).
- [19] B. Buijsse, E. R. Wouters, and W. J. van der Zande, *Phys. Rev. Lett.* **77**, 243 (1996).
- [20] C. W. Walter, P. C. Cosby, and H. Helm, *J. Chem. Phys.* **112**, 4621 (2000).
- [21] L. Dinu, Y. J. Picard, and W. J. van der Zande, *J. Chem. Phys.* **121**, 3058 (2004).
- [22] R. Ali, C. L. Cocke, M. L. A. Raphaelian, and M. Stockli, *Phys. Rev. A* **49**, 3586 (1994).
- [23] A. Hishikawa, A. Iwamae, and K. Yamanouchi, *Phys. Rev. Lett.* **83**, 1127 (1999).
- [24] K. Yamanouchi, *Science* **295**, 1659 (2002).
- [25] U. Müller, T. Eckert, M. Braun, and H. Helm, *Phys. Rev. Lett.* **83**, 2718 (1999).
- [26] T. Ergler, A. Rudenko, B. Feuerstein, K. Zrost, C. D. Schröter, R. Moshhammer, and J. Ullrich, *Phys. Rev. Lett.* **97**, 193001 (2006).
- [27] R. Dörner, H. Bräuning, O. Jagutzki, V. Mergel, M. Achler, R. Moshhammer, J. M. Feagin, T. Osipov, A. Bräuning-Demian, L. Spielberger, J. H. McGuire, M. H. Prior, N. Berrah, J. D. Bozek, C. L. Cocke, and H. Schmidt-Böcking, *Phys. Rev. Lett.* **81**, 5776 (1998).
- [28] Note that the references in the Introduction represent only a small portion of the available material and are examples meant to guide the reader to some of the earliest and most pertinent work in the respective areas.
- [29] J. Ullrich, R. Moshhammer, R. Dörner, O. Jagutzki, V. Mergel, H. Schmidt-Böcking, and L. Spielberger, *J. Phys. B: At. Mol. Phys.* **30**, 2917 (1997).
- [30] R. R. Dörner, V. Mergel, O. Jagutzki, L. Spielberger, J. Ullrich, R. Moshhammer, and H. Schmidt-Böcking, *Phys. Rep.* **330**, 95 (2000).
- [31] J. Ullrich, R. Moshhammer, A. Dorn, R. Dörner, L. P. H. Schmidt, and H. Schmidt-Böcking, *Rep. Prog. Phys.* **66**, 1463 (2003).
- [32] M. Pitzer, M. Kunitski, A. S. Johnson, T. Jahnke, H. Sann, F. Sturm, L. P. H. Schmidt, H. Schmidt-Böcking, R. Dörner, J.

- Stohner, J. Kiedrowski, M. Reggelin, S. Marquardt, A. Schießer, R. Berger, and M. S. Schöffler, *Science* **341**, 1096 (2013).
- [33] P. Herwig, K. Zawatzky, M. Grieser, O. Heber, B. Jordon-Thaden, C. Krantz, O. Novotný, R. Repnow, V. Schurig, D. Schwalm, Z. Vager, A. Wolf, O. Trapp, and H. Kreckel, *Science* **342**, 1084 (2013).
- [34] H. Ibrahim, B. Wales, S. Beaulieu, B. E. Schmidt, N. Thiré, E. P. Fowe, É. Bisson, C. T. Hebeisen, V. Wanie, M. Giguère, J.-C. Kieffer, M. Spanner, A. D. Bandrauk, J. Sanderson, M. S. Schuurman, and F. Légaré, *Nat. Commun.* **5**, 4422 (2014).
- [35] D. Zajfman and Z. Amitay, *Phys. Rev. A* **52**, 839 (1995).
- [36] D. Zajfman, Z. Amitay, C. Broude, P. Forck, B. Seidel, M. Grieser, D. Habs, D. Schwalm, and A. Wolf, *Phys. Rev. Lett.* **75**, 814 (1995).
- [37] J. R. Peterson, A. Le Padellec, H. Danared, G. H. Dunn, M. Larsson, A. Larson, R. Peverall, C. Strömholm, S. Rosén, M. af Ugglas, and W. J. van der Zande, *J. Chem. Phys.* **108**, 1978 (1998).
- [38] S. Datz, R. Thomas, S. Rosén, M. Larsson, A. M. Derkatch, F. Hellberg, and W. van der Zande, *Phys. Rev. Lett.* **85**, 5555 (2000).
- [39] R. D. Thomas, F. Hellberg, A. Neau, S. Rosén, M. Larsson, C. R. Vane, M. E. Bannister, S. Datz, A. Petrigiani, and W. J. van der Zande, *Phys. Rev. A* **71**, 032711 (2005).
- [40] D. Kella, P. J. Johnson, H. B. Pedersen, L. Vejby-Christensen, and L. H. Andersen, *Phys. Rev. Lett.* **77**, 2432 (1996).
- [41] L. H. Andersen, P. J. Johnson, D. Kella, H. B. Pedersen, and L. Vejby-Christensen, *Phys. Rev. A* **55**, 2799 (1997).
- [42] L. Vejby-Christensen, D. Kella, H. B. Pedersen, and L. H. Andersen, *Phys. Rev. A* **57**, 3627 (1998).
- [43] C. Dimopoulou, R. Moshhammer, D. Fischer, C. Höhr, A. Dorn, P. D. Fainstein, J. R. Crespo López Urrutia, C. D. Schröter, H. Kollmus, R. Mann, S. Hagmann, and J. Ullrich, *Phys. Rev. Lett.* **93**, 123203 (2004).
- [44] A. M. Saylor, P. Q. Wang, K. D. Carnes, B. D. Esry, and I. Ben-Itzhak, *Phys. Rev. A* **75**, 063420 (2007).
- [45] M. J. Besnard-Ramage, P. Morin, T. Lebrun, I. Nenner, M. J. Hubin-Franskin, J. Delwiche, P. Lablanquie, and J. H. D. Eland, *Rev. Sci. Instrum.* **60**, 2182 (1989).
- [46] M. Takahashi, J. P. Cave, and J. H. D. Eland, *Rev. Sci. Instrum.* **71**, 1337 (2000).
- [47] R. Thissen, J. Delwiche, J. M. Robbe, D. Duflo, J. P. Flament, and J. H. D. Eland, *J. Chem. Phys.* **99**, 6590 (1993).
- [48] T. Weber, M. Weckenbrock, M. Balsler, L. Schmidt, O. Jagutzki, W. Arnold, O. Hohn, M. Schöffler, E. Arenholz, T. Young, T. Osipov, L. Foucar, A. De Fanis, R. Díez Muiño, H. Schmidt-Böcking, C. L. Cocke, M. H. Prior, and R. Dörner, *Phys. Rev. Lett.* **90**, 153003 (2003).
- [49] T. Osipov, C. L. Cocke, M. H. Prior, A. Landers, T. Weber, O. Jagutzki, L. Schmidt, H. Schmidt-Böcking, and R. Dörner, *Phys. Rev. Lett.* **90**, 233002 (2003).
- [50] I. Ben-Itzhak, P. Wang, J. Xia, A. M. Saylor, M. A. Smith, J. Maseberg, K. D. Carnes, and B. D. Esry, *Nucl. Instrum. Methods Phys. Res., Sect. B* **233**, 56 (2005).
- [51] Note that atomic units are used unless otherwise noted.
- [52] S. Zeller *et al.*, *Proc. Natl. Acad. Sci. USA* **113**, 14651 (2016).
- [53] J. McKenna, A. M. Saylor, B. Gaire, N. G. Johnson, K. D. Carnes, B. D. Esry, and I. Ben-Itzhak, *Phys. Rev. Lett.* **103**, 103004 (2009).
- [54] A. M. Saylor, J. McKenna, B. Gaire, N. G. Kling, K. D. Carnes, and I. Ben-Itzhak, *Phys. Rev. A* **86**, 033425 (2012).
- [55] T. Graber, E. P. Kanter, J. Levin, D. Zajfman, Z. Vager, and R. Naaman, *Phys. Rev. A* **56**, 2600 (1997).
- [56] J. Levin, D. Kella, and Z. Vager, *Phys. Rev. A* **53**, 1469 (1996).
- [57] D. Talbi and R. P. Saxon, *J. Chem. Phys.* **89**, 2235 (1988).
- [58] J. McKenna, A. M. Saylor, B. Gaire, N. G. Kling, B. D. Esry, K. D. Carnes, and I. Ben-Itzhak, *New J. Phys.* **14**, 103029 (2012).
- [59] A. M. Saylor, J. McKenna, B. Gaire, N. G. Kling, K. D. Carnes, B. D. Esry, and I. Ben-Itzhak, *J. Phys. B: At. Mol. Phys.* **47**, 031001 (2014).
- [60] J. Tennyson, *Rep. Prog. Phys.* **58**, 421 (1995).
- [61] O. Friedrich, A. Alijah, Z. R. Xu, and A. J. C. Varandas, *Phys. Rev. Lett.* **86**, 1183 (2001).
- [62] J. C. López Vieyra and A. V. Turbina, *Phys. Rev. A* **66**, 023409 (2002).
- [63] T. R. Geballe and T. Oka, *Nature (London)* **384**, 334 (1996).
- [64] B. J. McCall, A. J. Huneycutt, R. J. Saykally, T. R. Geballe, N. Djuric, G. H. Dunn, J. Semaniak, O. Novotny, A. Al-Khalili, A. Ehlerding, F. Hellberg, S. Kalhori, M. Larsson, A. Neau, R. Thomas, and F. Osterdahl, *Nature (London)* **422**, 500 (2003).
- [65] T. Oka, *Proc. Natl. Acad. Sci. USA* **103**, 12235 (2006).
- [66] B. J. McCall, *Philos. Trans. R. Soc. London, Ser. A* **358**, 2385 (2000).
- [67] V. G. Anicich and J. H. Futrell, *Int. J. Mass Spectrom. Ion Processes* **55**, 189 (1984).
- [68] N. Johnson, Controlling the dynamics of electrons and nuclei in ultrafast strong laser fields, Dissertation, Kansas State University, 2013.